

**Supporting information for:**

## **Acetone-derived luminescent polymer dots: a facile and low-cost synthesis leads to remarkable photophysical properties**

Sebastian G. Mucha<sup>a</sup>, Lucyna Firlej<sup>a</sup>, Jean-Louis Bantignies<sup>a</sup>, Andrzej Żak<sup>b</sup>, Marek Samoć<sup>c</sup>,  
Katarzyna Matczyszyn<sup>c\*</sup>

<sup>a</sup>*Laboratoire Charles Coulomb, University of Montpellier, CNRS, Montpellier 34095, France.*

<sup>b</sup>*Electron Microscopy Laboratory, Faculty of Mechanical Engineering, Wrocław University of Science and Technology, Wyb. Wyspiańskiego 27, 50-370 Wrocław, Poland.*

<sup>c</sup>*Advanced Materials Engineering and Modelling Group, Wrocław University of Science and Technology, Wyb. Wyspiańskiego 27, 50-370 Wrocław, Poland.*

**Keywords:** polymer dots, acetone, greenish-blue photoluminescence

**Corresponding author:** \*Katarzyna Matczyszyn (katarzyna.matczyszyn@pwr.edu.pl)

## Table of contents:

Materials.....	3
Synthesis of C-1Na and C-2Na (NaOH-based PDs) – detailed protocol.....	3
Synthesis of C-1K and C-2K (KOH-based PDs).....	4
Techniques.....	4
Structural characterization .....	4
Steady-state spectroscopy.....	5
Time-resolved spectroscopy .....	6
Results .....	7
Synthesis monitoring.....	8
TEM imaging and size distributions.....	10
XRD diagrams .....	11
ATR-FTIR spectra .....	12
TR-FTIR spectra.....	15
Raman spectra .....	16
XPS spectra .....	17
Extinction, excitation and emission spectra .....	21
Absolute photoluminescence quantum yield.....	25
Photoluminescence decay curves .....	26
References: .....	34

## Materials

Acetone (Ac<sub>2</sub>O, 99.9%), acetylacetone (99.0%), 2,2-dimethoxy-2-phenylacetophenone (AP, 99.0%), potassium hydroxide (KOH, ~98%), sodium hydroxide (NaOH, ~98%), concentrated hydrochloric acid (HCl, 36%), 1-butanol (99.9%), and 2-propanol (99.9%), were purchased from Sigma-Aldrich Co. LLC. Milli-Q ultrapure water was provided by Milli-Q Integral Water Purification System. All chemicals were used throughout the experiments without further purification processes.

## Synthesis of C-1Na and C-2Na (NaOH-based PDs) – detailed protocol

According to the modified Hou's protocol (**Scheme S1.**)<sup>1</sup> 8.1 g of NaOH powder (0.2 mol, 1.0 eq, Sigma-Aldrich, ~98%) was loaded into 100 mL three-neck round-bottom flask equipped with a magnetic stirrer, reflux, and a water bath. Afterwards, 40.4 mL of ultrapure acetone (0.55 mol, 2.75 eq, Sigma-Aldrich, 99.9%) was briefly injected and the as-obtained reaction mixture was refluxed with vigorous stirring (400 rpm) for 72 hours at ambient conditions, preventing acetone evaporation. During the fabrication process, reaction solution has changed form from colorless transparent to orange liquid, resulting finally in a dark-brown and dense mixture. To stop the synthesis of PDs, a certain amount of 1M HCl was incorporated into the reaction mixture to neutralize unreacted NaOH, adjusting pH to be 7.02. The two-phase product was supplied by 2x20 mL aliquots of n-butanol along with 2x20 mL aliquots of pure water and then extracted twice, resulting in hydrophilic (**C-1Na**) and hydrophobic (**C-2Na**) fractions of PDs. The thus-obtained products were dried in a lyophilizer or using a rotary evaporator. Subsequently, water-

soluble PDs were washed with isopropanol and filtered to discard NaCl salt and placed into the freeze-drier. In consequence, brown powders were received.

## Synthesis of C-1K and C-2K (KOH-based PDs)

Furthermore, KOH-based PDs were also fabricated by following the same synthesis route, wherein KOH was used as a reaction catalyst rather than NaOH, while keeping the same precursors ratio (1:2.75). Similar to the above preparation avenue, hydrophilic and hydrophobic PDs were obtained, which are denoted as **C-1K** and **C-2K**, respectively. As-prepared PDs were re-dispersed in water and methanol/n-butanol and used for further experiments without any post-synthesis treatments.

## Techniques

### Structural characterization

Solid-state attenuated-total reflectance Fourier-transform infrared (ATR-FTIR) spectra in the middle infrared range (MIR: 4000-400  $\text{cm}^{-1}$ ) of each PDs sample were taken with a Nicolet iS10 FTIR spectrometer (Thermo Scientific) using KBr beam splitter, pyroelectric DTGS detector and black body source. Alternatively, MIR FTIR spectra were also measured on an IFS 66v/S spectrometer (Bruker), operating in transmission mode (KBr beam splitter, pyroelectric DTGS detector and black body source). Prior to this experiment in TR mode, each sample was mixed with KBr in pellet and dried to reduce the amount of water, samples were probed without dilution in ATR-FTIR mode. X-ray diffraction patterns were acquired on a home-made system (a copper  $\text{K}\alpha$  anode,  $\lambda_{\text{beam}} = 0.15418 \text{ nm}$ ). Transmission electron microscopy (TEM) samples were prepared by applying a 3  $\mu\text{l}$  drop of 0.5 mg/mL solution to the standard carbon on copper grid and air-

drying. Imaging single PDs near the borders of the densest areas was conducted on a W-filament Hitachi H-800 conventional TEM instrument, working at 150 kV accelerating voltage. To determine precisely the size distribution of PDs, 150 nanoobjects from each sample were taken into account. Besides, PDs were also investigated by the Static Light Scattering (SLS) technique on a Multi-angle dynamic and static light scattering instrument Photocor Complex with a TEC stabilized diode laser (638 nm, 25 mW) oriented at 90° and 150°, resulting in hydrodynamic diameters of our PDs. The XPS spectra were measured at the high-vacuum conditions with a hemispheric analyser VG SCIENTA using a monochromatic X-ray source Al K $\alpha$  excitation ( $E = 1486.6$  eV, 450 mW, 30mA, MX650, VG Scienta) and a He lamp (UVS 40A, Prevac). The interpretation of as-obtained data was carried out according to the XPS data collection and articles on carbon nanomaterials. Raman spectroscopy measurements were performed for each sample in powder and dispersion forms on two different experimental setups: i) the RF6 100/S Bruker spectrometer, operating at 1064 nm, and ii) a home-built system that consists of a Model 3900S laser system ( $\lambda_{\text{beam}} = 750$  nm) and iHR 550 Spectrometer. Changes in pH values were monitored by employing a Mettler Toledo instrument (SevenCompact Series).

### **Steady-state spectroscopy**

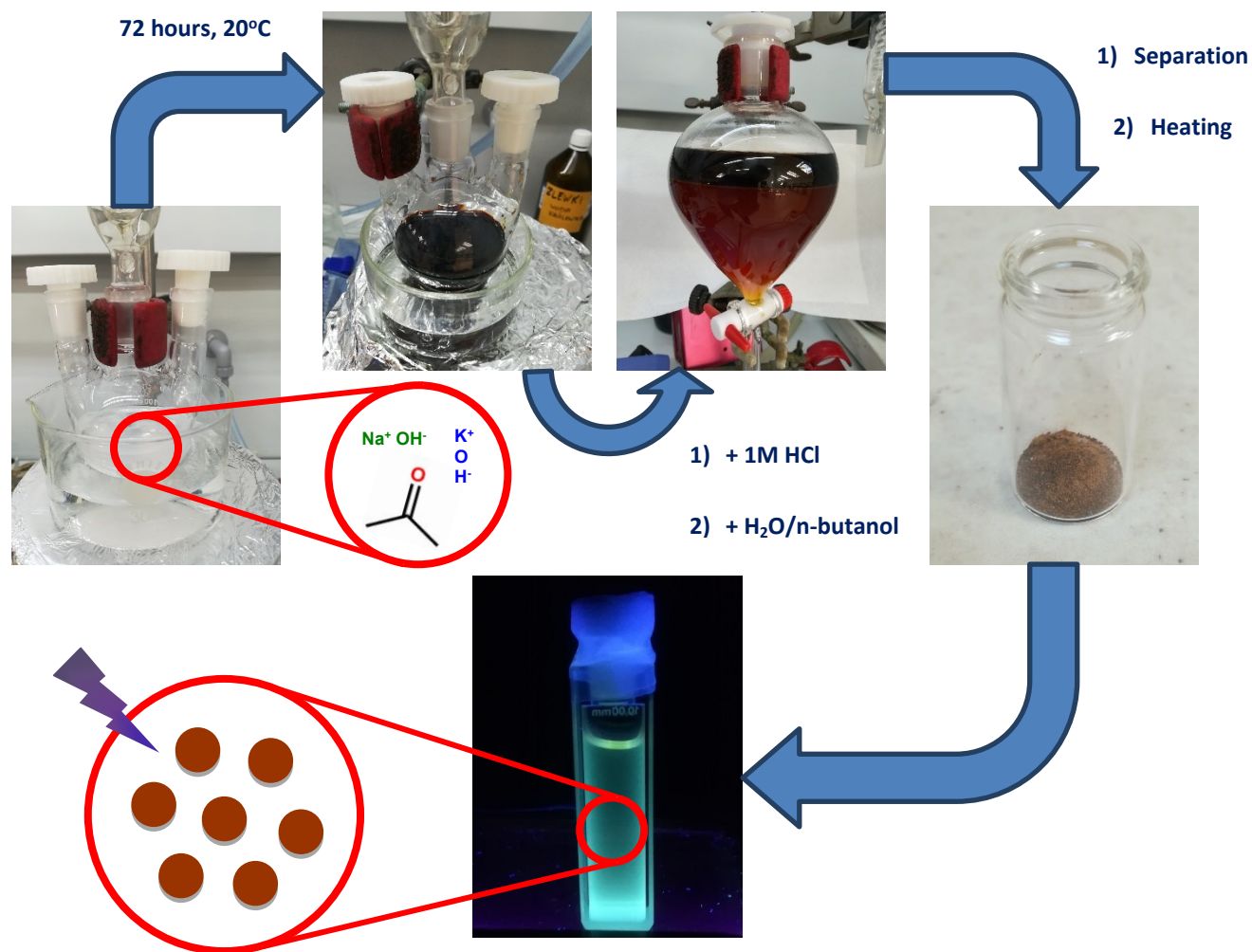
The UV-Vis extinction spectra were recorded in a wide wavelength range (270 nm – 700 nm) on a JASCO V-730 spectrophotometer while emission and excitation spectra of PDs were acquired on a FluoroMax-4 spectrofluorimeter (Horiba Jobin Yvon) with 5.0 nm excitation/emission slits width. The two-dimensional excitation-emission topographical maps were generated by scanning excitation and emission spectra in wide spectral windows, being 280 nm - 600 nm for excitation wavelengths and 300 nm - 800 nm for emission wavelengths. A

conventional quartz cuvette (10 × 10 × 45 mm) was used for the above spectroscopic measurements. To determine absolute photoluminescence quantum yields (PLQYs), emission spectra and changes in the excitation peak were collected on a custom-built setup, consisting of an integrating sphere, a FLS 980 Edinburgh Instruments spectrometer, and a BDL - 375 - SMN Picosecond Laser Diode (20 MHz, 377 nm) as an excitation source.

### **Time-resolved spectroscopy**

The photoluminescence decay profiles of PDs were measured through a conventional time-correlated single-photon counting (TCSPC) setup, containing a BDL - 375 - SMN Picosecond Laser Diode (20 MHz, 377 nm), an Acton SpectraPro SP-2300 monochromator (Princeton Instruments), and a high-speed hybrid detector HPM-100-50 (Becker&Hickl GmbH) which was controlled by a DCC-100 card.

## Results



**Scheme S1.** Schematic representation illustrating the formation of blue-emitting PDs through alkali-mediated aldol reaction in anhydrous conditions.

## Synthesis monitoring

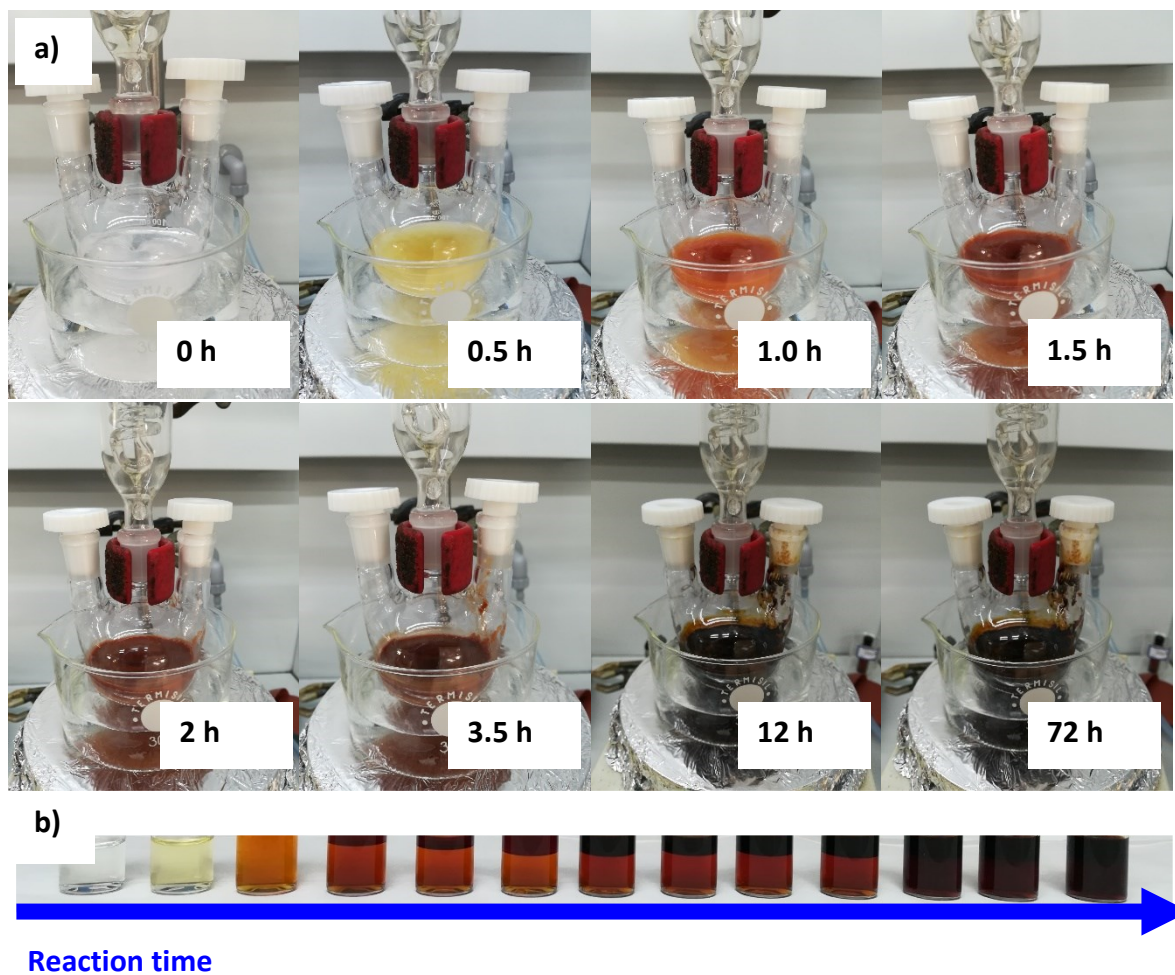


**Figure S1. a)** The changes in colour of reaction mixture as function of time, indicating progress in the synthesis of NaOH-like PDs. **b)** The evolution of hydrophobic (top) and hydrophilic (bottom) phases during synthesis process. Prior to spectroscopic analysis, reactions were stopped in each sample by treating with 1M HCl to adjust pH  $\sim$ 7.0 and filled with water until volume was 8 mL.

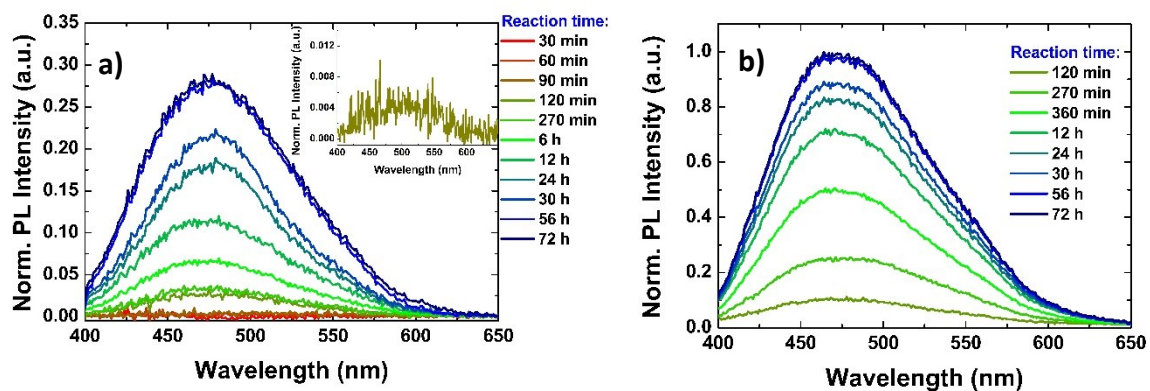


**Figure S2.** The progress in the fabrication of PDs as an evolution of photoluminescence spectra, for hydrophilic **(a)** and hydrophobic **(b)** fractions of NaOH-based PDs which were previously normalized with respect to the most intense scan. The legend in the panel indicates the reaction time.

## TEM imaging and size distributions

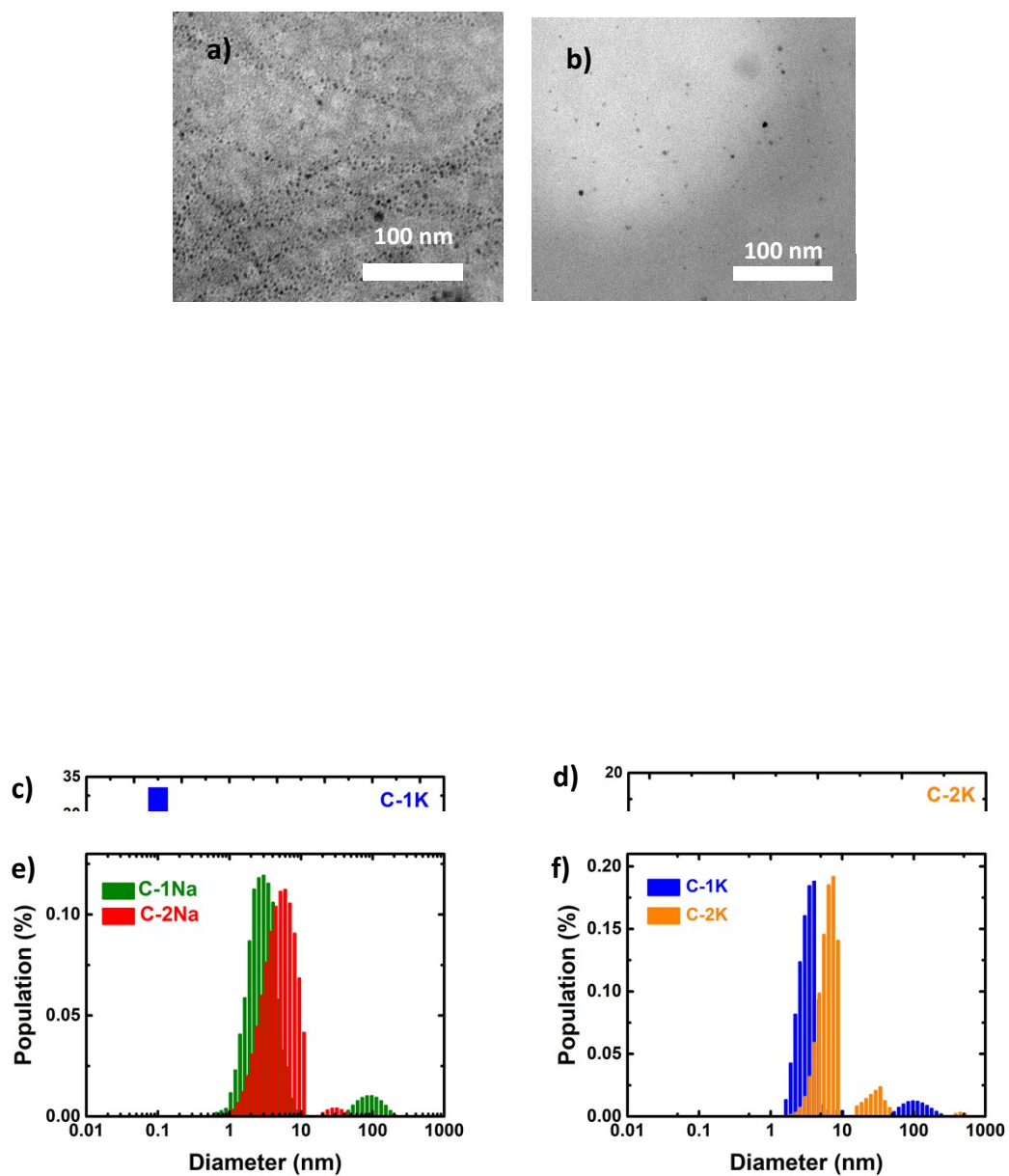


**Figure S3.** TEM images of the KOH-derived PDs (**a**, **b**) and their corresponding size distributions (**c**, **d**). The supplementary size distributions taken from SLS measurements (**e**, **f**).

## XRD diagrams

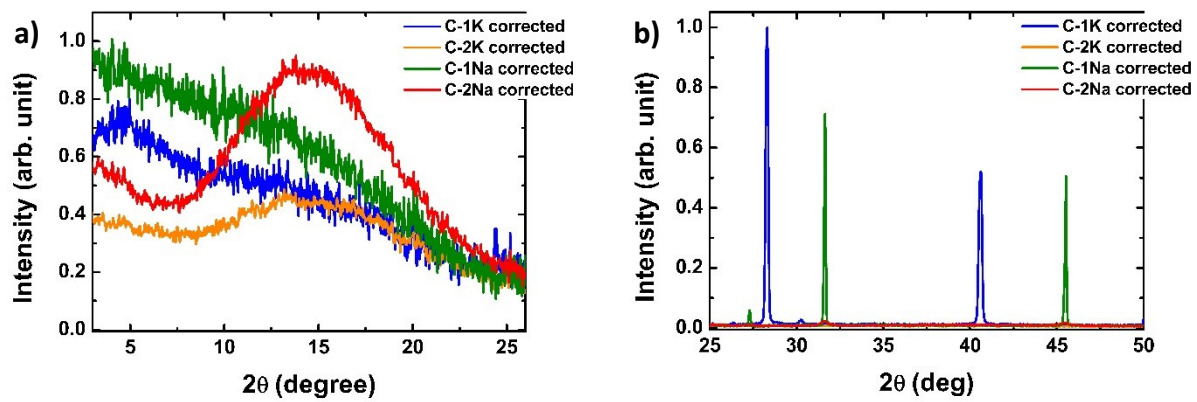


**Figure S4.** The XRD patterns of all four samples in two ranges  $2\theta$ , indicating amorphous phase in hydrophobic PDs (a) and the excess of salts in hydrophilic PDs (b).

## ATR-FTIR spectra

The particular chemical moieties in PDs were thoroughly identified, taking into account the

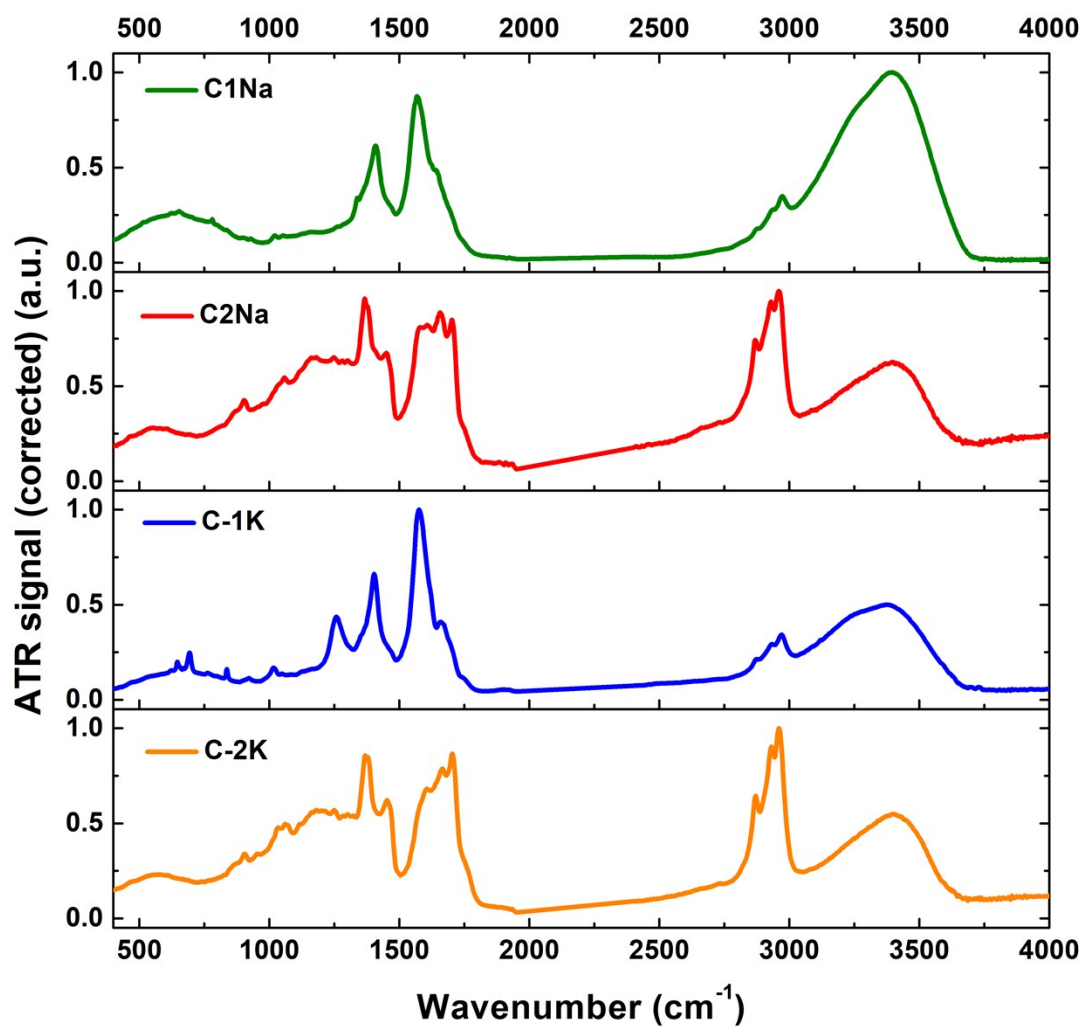
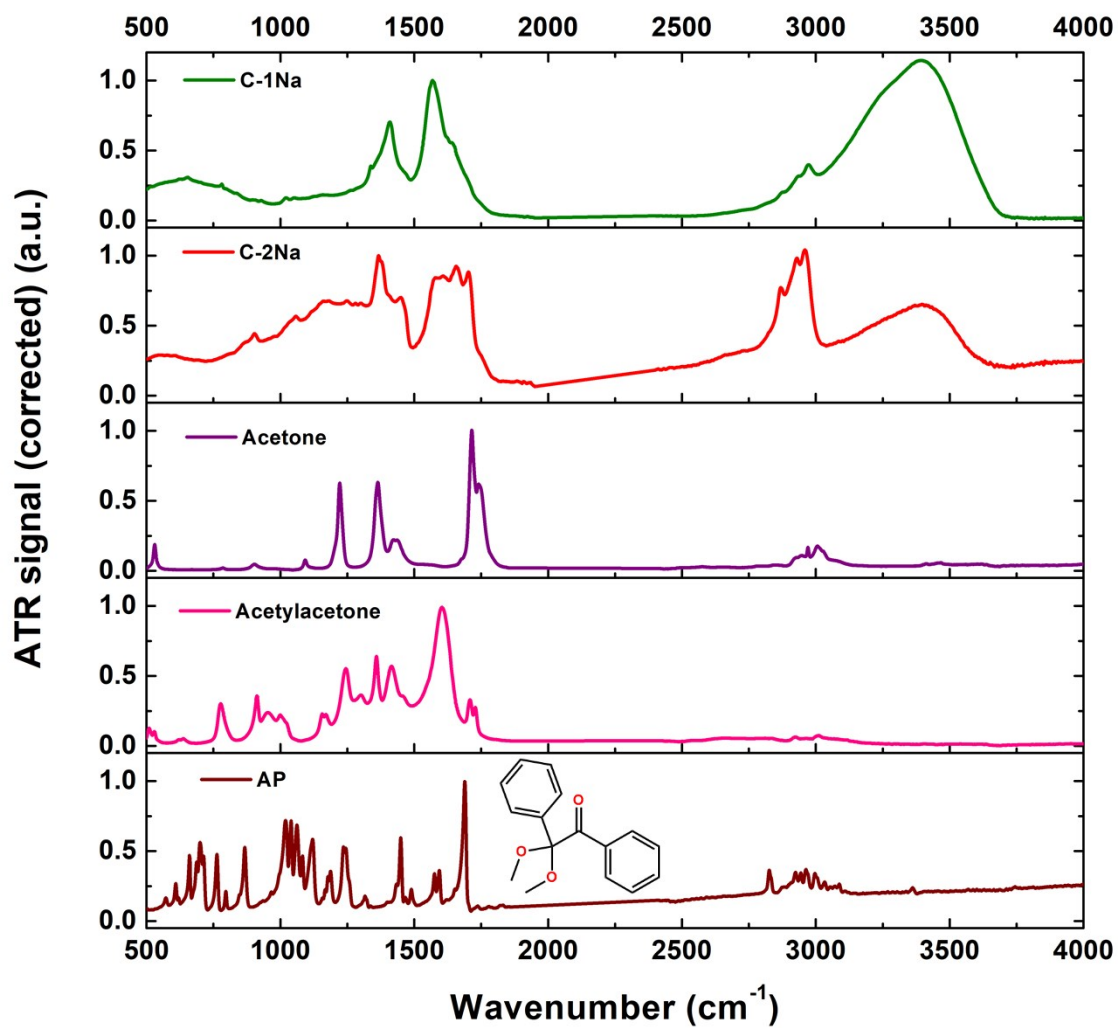


Figure S5. The ATR-FTIR spectra of all PDs.

analysis of complex organic molecules.<sup>2-6</sup>



**Figure S6.** The ATR-FTIR spectra of NaOH-based PDs and representative ketones (**AP** = 2,2-dimethoxy-2-phenylacetophenone).

**Table S1.** The most characteristic absorption peaks of PDs in the infrared regime, (+/- correspond to detection/absence of the peak).

Absorption range (cm <sup>-1</sup> )	Vibrations	Hydrophilic PDs	Hydrophobic PDs	Ref.
800-1320	e.g. C-C(=O)-C backbone stretching, C-C-O stretching C-H, C-O, O-H deformation	+	+	4, 7-11
1368, 1378	C-H bending (symmetric deformations)	-	+	5, 9
1403	C-O-C stretching	+	-	11
1451	methyl C-H bending (asymmetric deformations)	-	+	5, 9
1576	enol C=O stretching	+	-	3, 9, 12
1602, 1638	C=C stretching	-	+	3, 9-10
1620, 1656	C=C stretching	+	-	3, 7, 9, 13
1666	C=O/C=C stretching	-	+	1, 3, 9
1703	C=O stretching	-	+	1, 3, 9, 12-13
2655, 2704, 2725, 2800, 2839	enol O-H---H stretching	+	-	3, 9, 12, 14-15
2870	symmetric methyl C-H stretching	+	+	1, 5, 9, 16
2931	asymmetric methylene C-H stretching	+	+	5, 7, 9, 16
2960	asymmetric methyl C-H stretching	+	+	1, 5, 9
3401	O-H stretching (intermolecular hydrogen bonding)	+	+	4, 9-10, 17-18

## TR-FTIR spectra

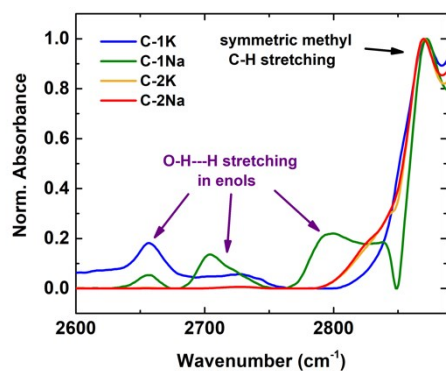


**Figure S7.** The TR-FTIR spectra of all PDs (2600 - 2890  $\text{cm}^{-1}$ ), normalized with respect to absorption peaks of symmetric methyl C-H stretching vibrations. The bands corresponding to O-H...H stretching vibrations are indicated by violet arrows.

**Table S2.** The ratios of absorbance values between -OH to  $-\text{CH}_3$  peaks which correspond to stretching vibrations.

Sample	Absorbance ratio ( $A_{\text{OH}}/A_{\text{CH}_3}$ )
<b>C-1Na</b>	0.80
<b>C-2Na</b>	0.36
<b>C-1K</b>	0.77
<b>C-2K</b>	0.37

## Raman spectra

No characteristic Raman peaks of graphitic CDs (at  $\sim 1350\text{ cm}^{-1}$  and  $\sim 1590\text{ cm}^{-1}$ ) were observed in the Raman spectra, in neither powder nor dispersion forms.<sup>19</sup> Nevertheless, the photoluminescence signal is well seen upon illumination with 750 nm and even 1064 nm (hydrophobic PDs).

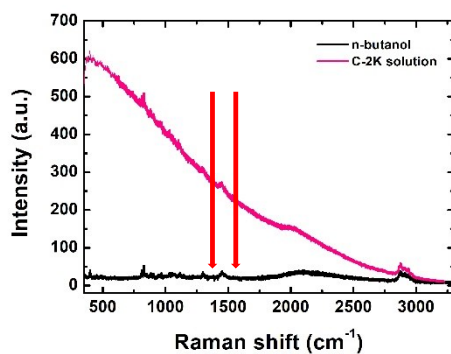


**Figure S8.** The Raman spectra of C-2K in n-butanol and pure solvent. All weak peaks are common for both samples. Expected signals are indicated by red arrows.

## XPS spectra

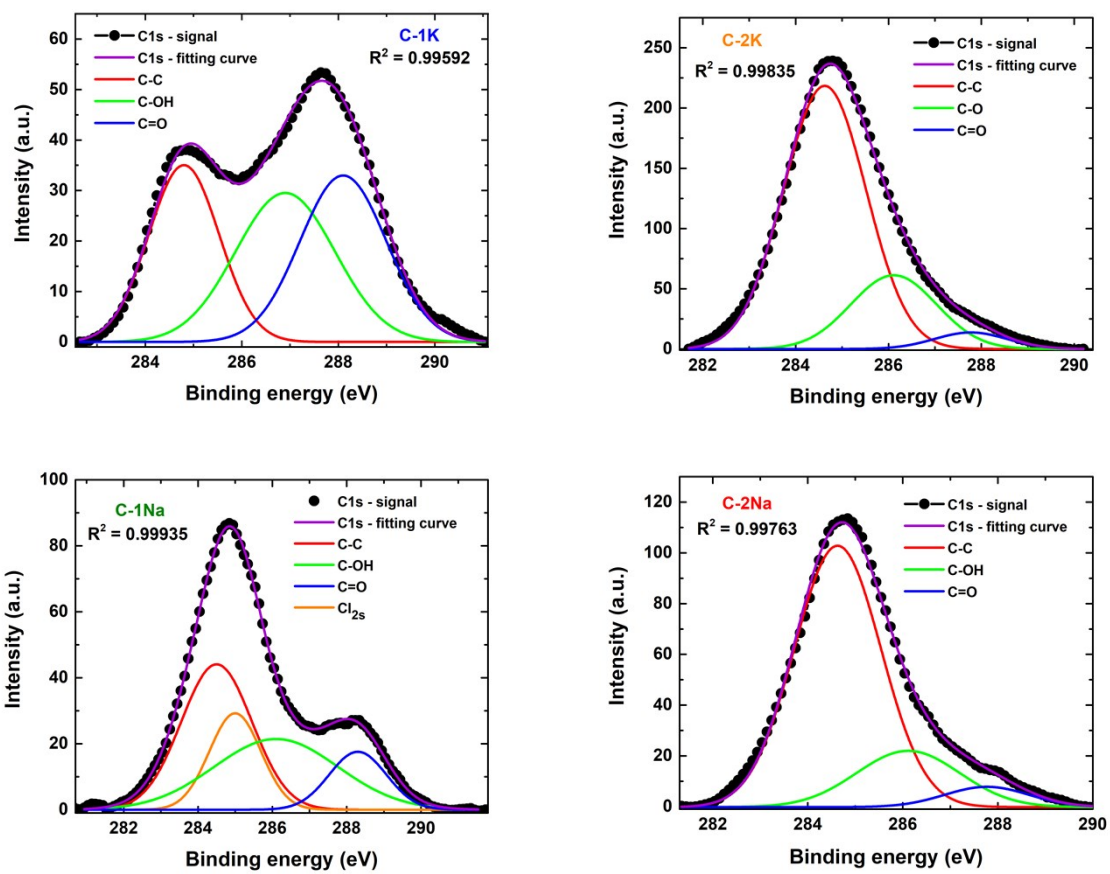


Figure S9. C1s XPS spectra.

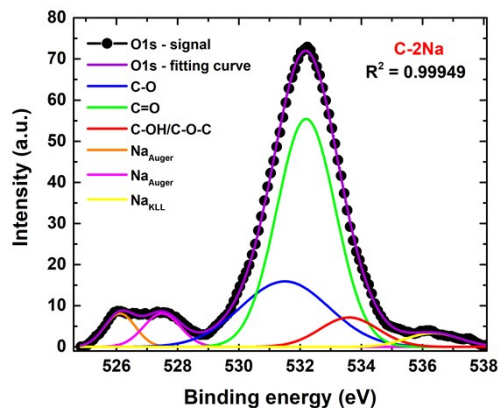
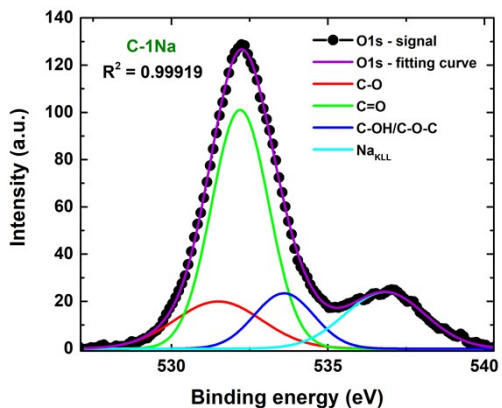
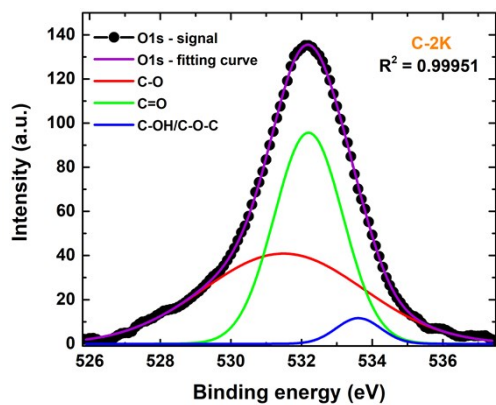
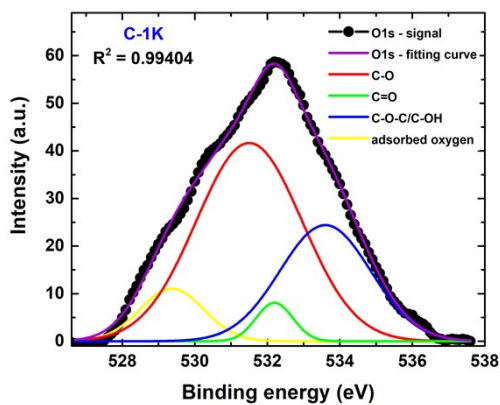


Figure S10. O1s XPS spectra.



**Figure S11.** The XPS spectra in the wide range of binding energy.



**Table S3.** The XPS characteristics after the Gaussian deconvolution of C1s and O1s peaks.

Signal	C1s			O1s		
Sample	C-C	C-OH	C=O	C-O	C=O	C-OH/C-O-C
<b>C-1Na</b>	46.0%	39.1%	14.8%	19.5%	64.9%	15.6%
<b>C-2Na</b>	75.8%	19.0%	5.2%	27.7%	64.1%	8.2%
<b>C-1K</b>	29.9%	35.6%	34.5%	63.7%	4.3%	32.0%
<b>C-2K</b>	74.3%	21.6%	4.1%	47.8%	48.4%	3.8%

## Extinction, excitation and emission spectra

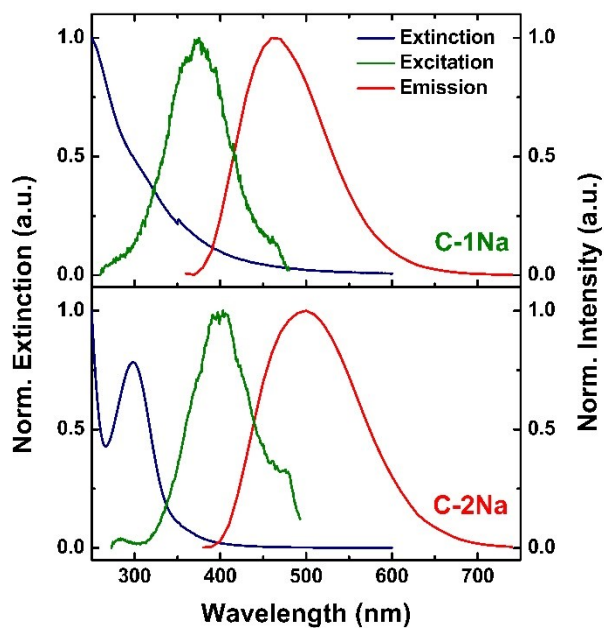


**Figure S12.** The normalized extinction (blue), representative excitation (green), and emission (red curve) spectra of NaOH-based PDs.

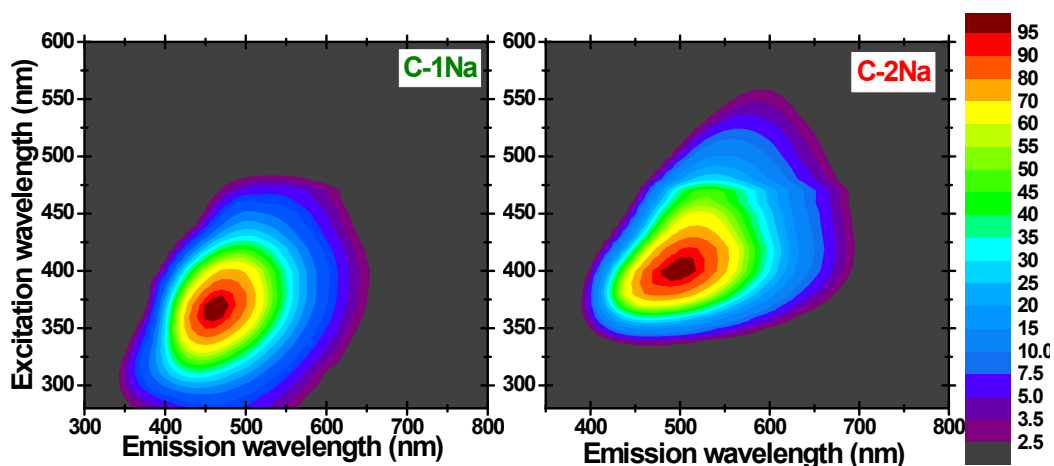


**Figure S13.** The photoluminescence excitation-emission map of NaOH-based PDs. The legend in the panel corresponds to normalized PL intensity.

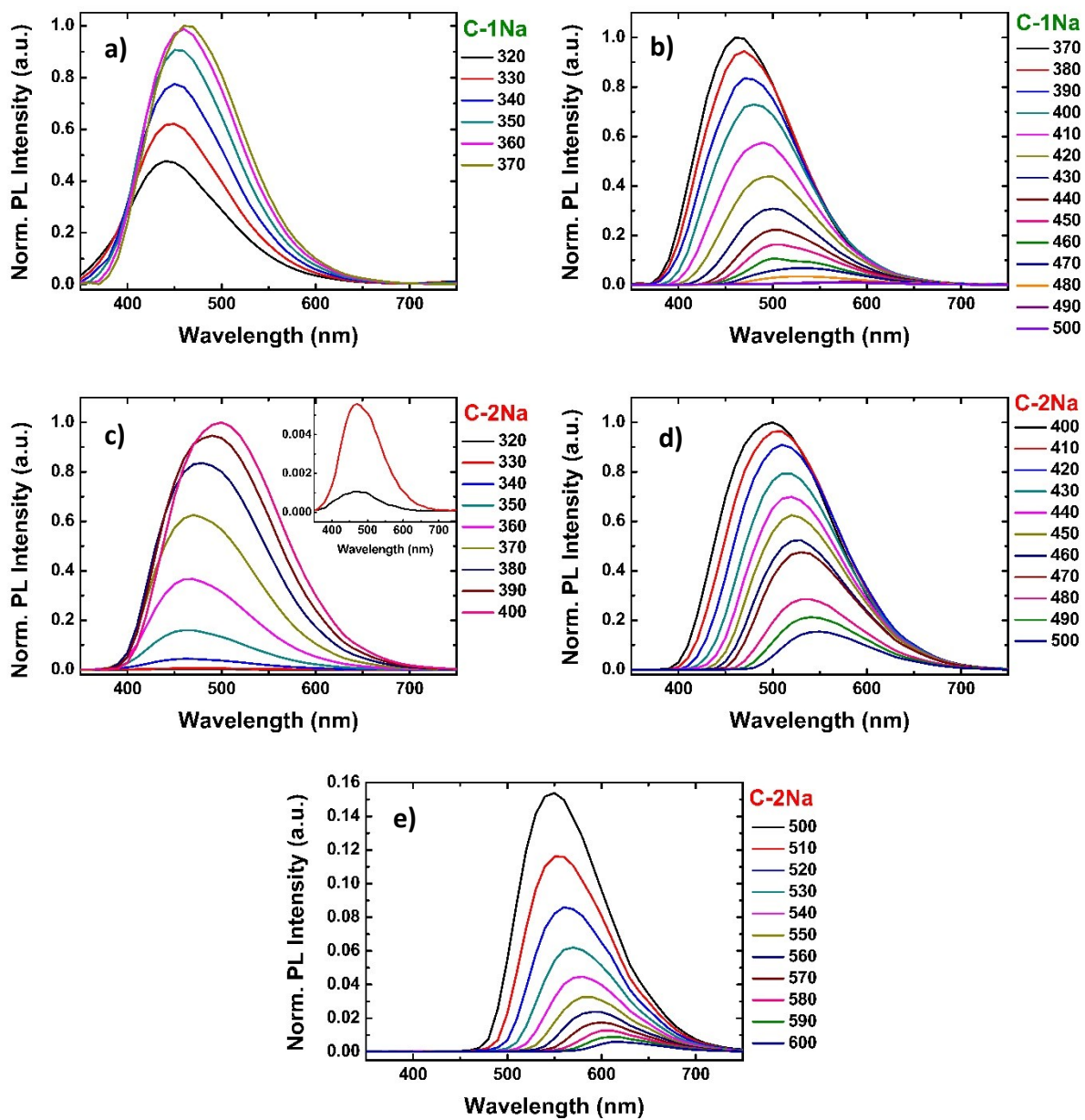


Figure S14. The excitation-dependent photoluminescence spectra of C-1Na and C-2Na.

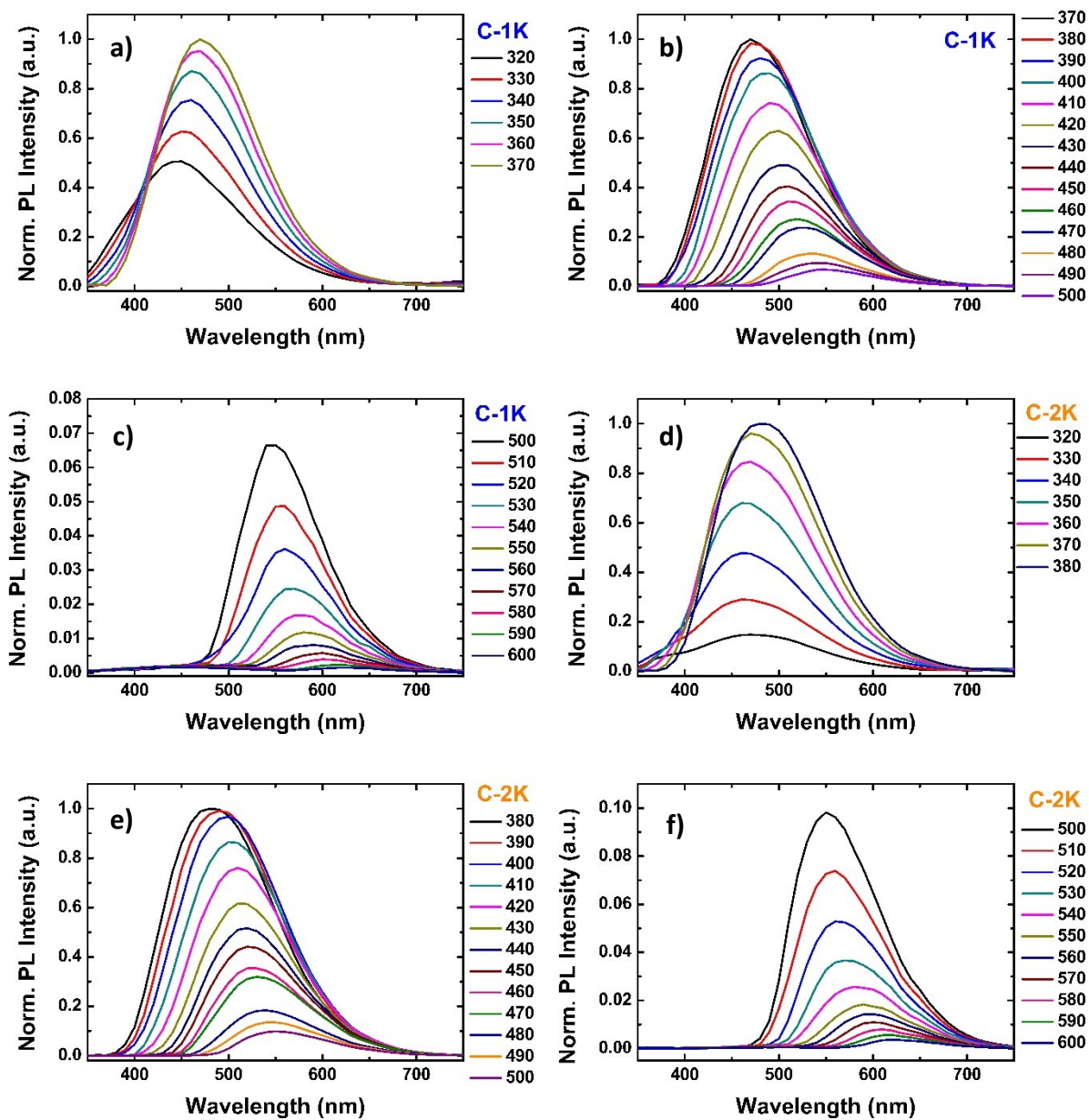
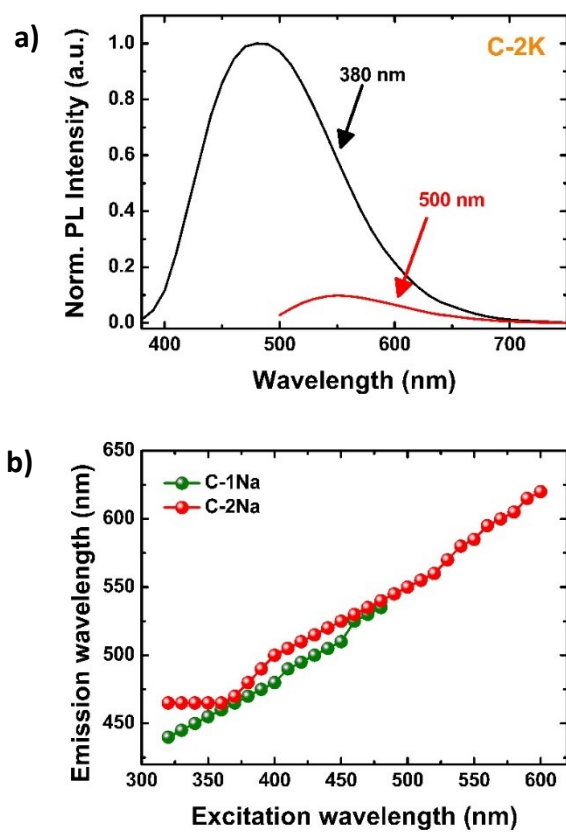


Figure S15. The excitation-dependent photoluminescence spectra of C-1K and C-2K.



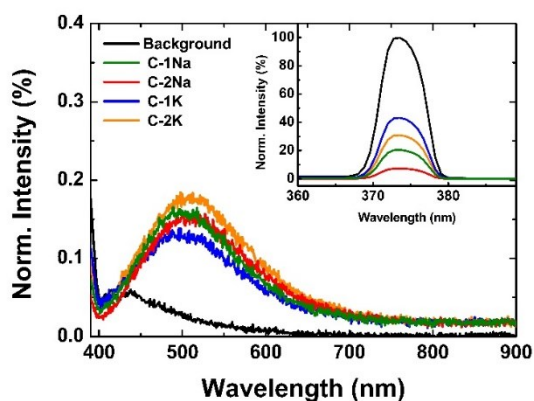
**Figure S16.** a) The normalized emission spectra of **C-2K** after excitation with 380 nm and 500 nm. b) The relation between emission and excitation maxima of NaOH-based PDs.

## Absolute photoluminescence quantum yield

The absolute photoluminescence quantum yields (PLQYs) were determined, so as to quantify thoroughly the real ability of the PDs to emit photoluminescence, taking into account the integrated photoluminescence intensity and the integrated intensity of incident light in the absence and presence of analyzed sample, as shown below:<sup>20-21</sup>

$$PLQY = \frac{S_2 - S_3}{S_0 - S_1}$$

where **PLQY** denotes the calculated value of PLQY (%),  $S_2$  represents the integrated PL intensity arising from sample (a.u.),  $S_0$  and  $S_1$  denote the integrated intensity of an excitation light in the



absence and presence of a sample (a.u.), respectively,  $S_3$  is the background (a.u.);

In fact, the direct approach to determine PLQY values is more accurate than comparative method, relying on comparison of plots between sample and reference, which is commonly used for various PDs. It should be noted that the direct determination of PLQY allows one to collect

**Figure S17.** The photoluminescence spectra of PDs collected by the integrating sphere and normalized with respect to the excitation beam. Inset represents changes in the excitation beam intensity in the presence and absence of

fully the emission light and rule out several errors, such as self-quenching, influence of light scattering during absorption measurements, and the error that appears for reference sample.

### **Photoluminescence decay curves**

Photoluminescence decay traces of individual hydrophilic and hydrophobic fractions of our PDs were fitted with tri-exponential function, as follows:

$$I(t) = A_1 \cdot \exp\left(-\frac{t}{\tau_1}\right) + A_2 \cdot \exp\left(-\frac{t}{\tau_2}\right) + A_3 \cdot \exp\left(-\frac{t}{\tau_3}\right)$$

where **I(t)** represents the photoluminescence intensity (a.u.), **t** denotes time (ns),  **$\tau_1$** ,  **$\tau_2$** ,  **$\tau_3$**  are lifetime components, and **A<sub>1</sub>**, **A<sub>2</sub>**, and **A<sub>3</sub>** are the relative decay amplitudes for the corresponding terms in the decay function.

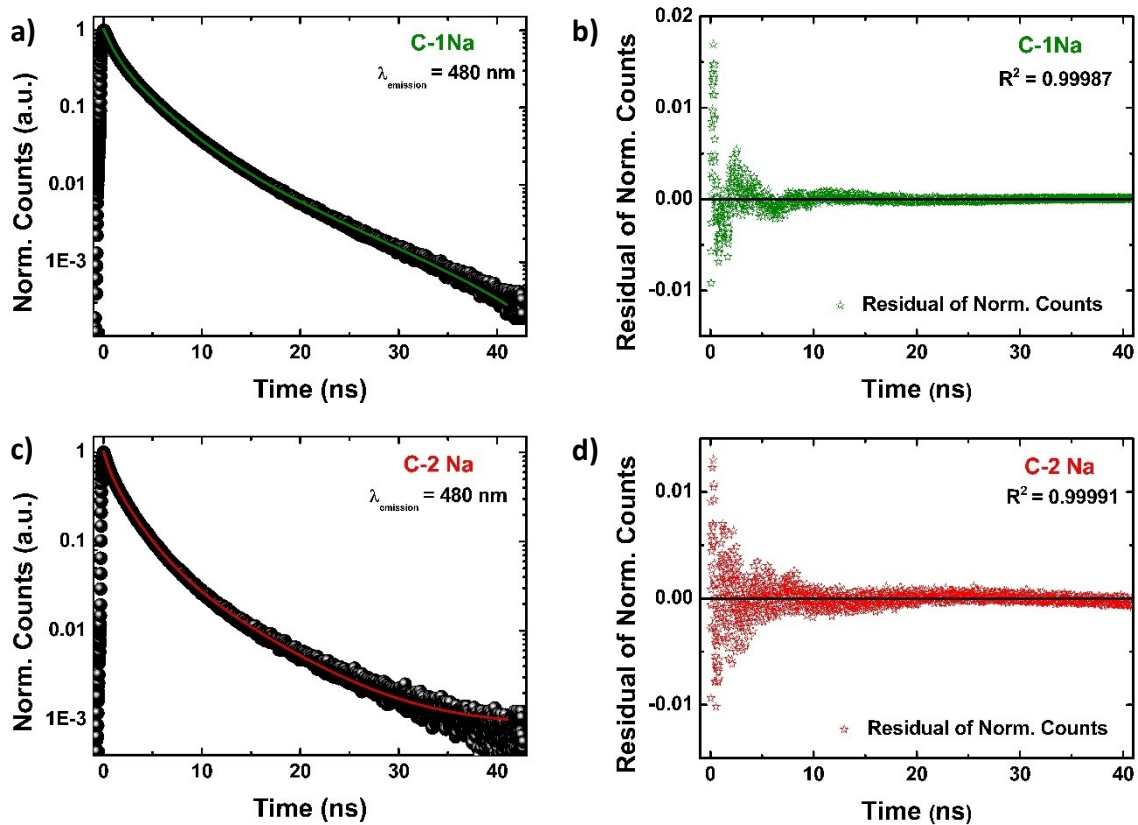


**Figure S18.** The photoluminescence decay profiles of NaOH-based PDs recorded at 480 nm (left panel) and their corresponding plots of residuals (right panel).

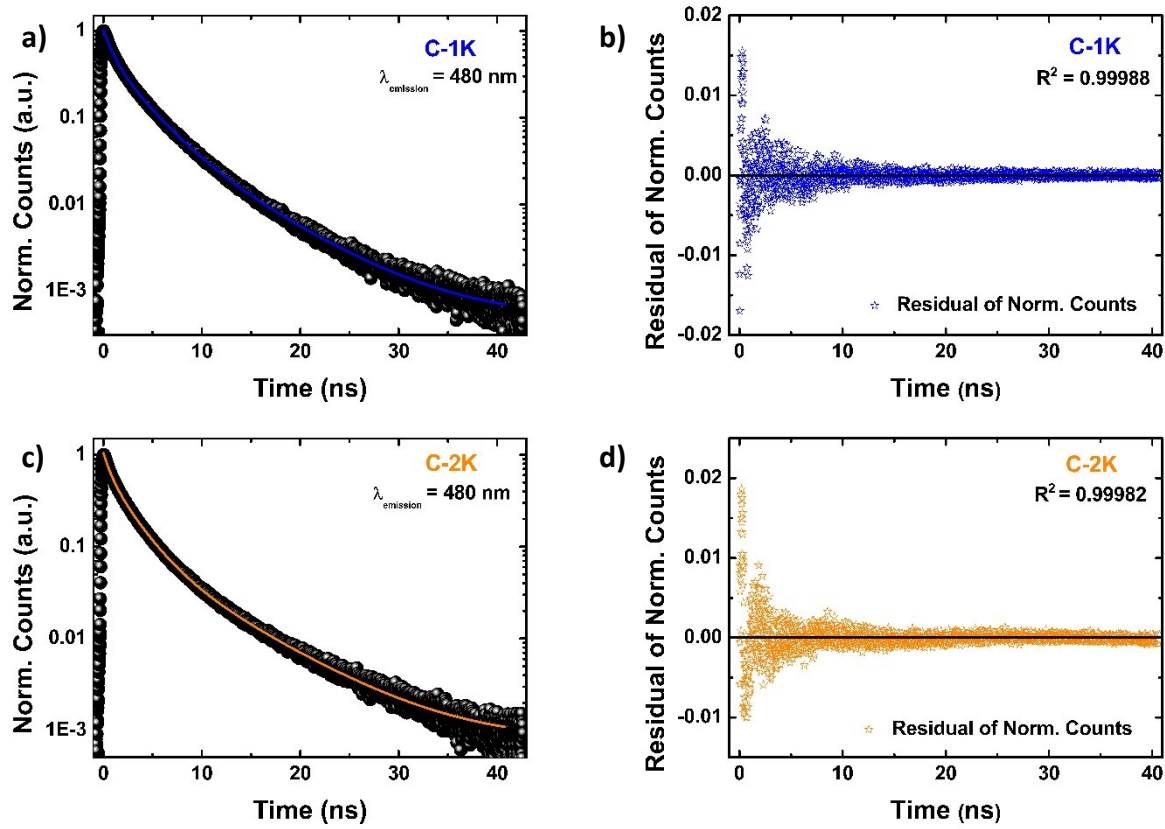


**Figure S19.** The photoluminescence decay profiles of KOH-based PDs recorded at 480 nm (left panel) and their corresponding plots of residuals (right panel).

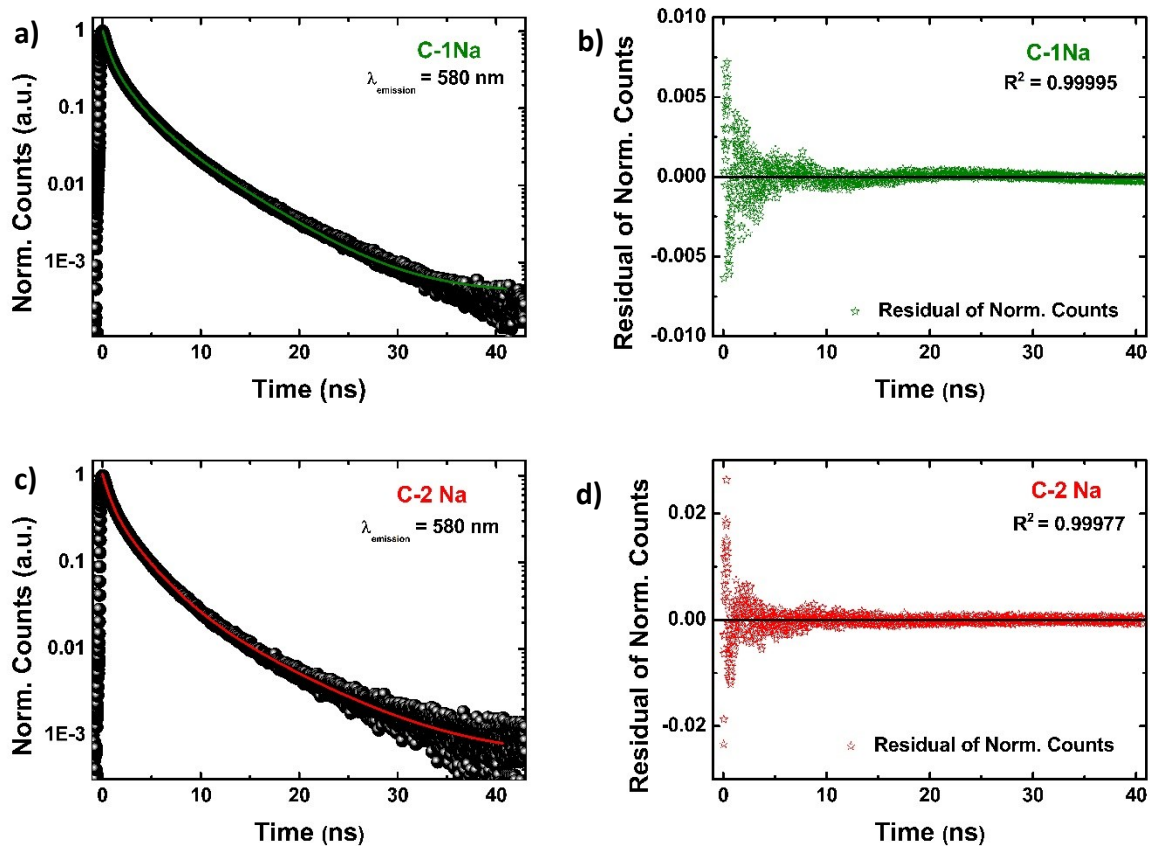


**Figure S20.** The photoluminescence decay traces of NaOH-based PDs recorded at 580 nm (left panel) and their corresponding plots of residuals (right panel).

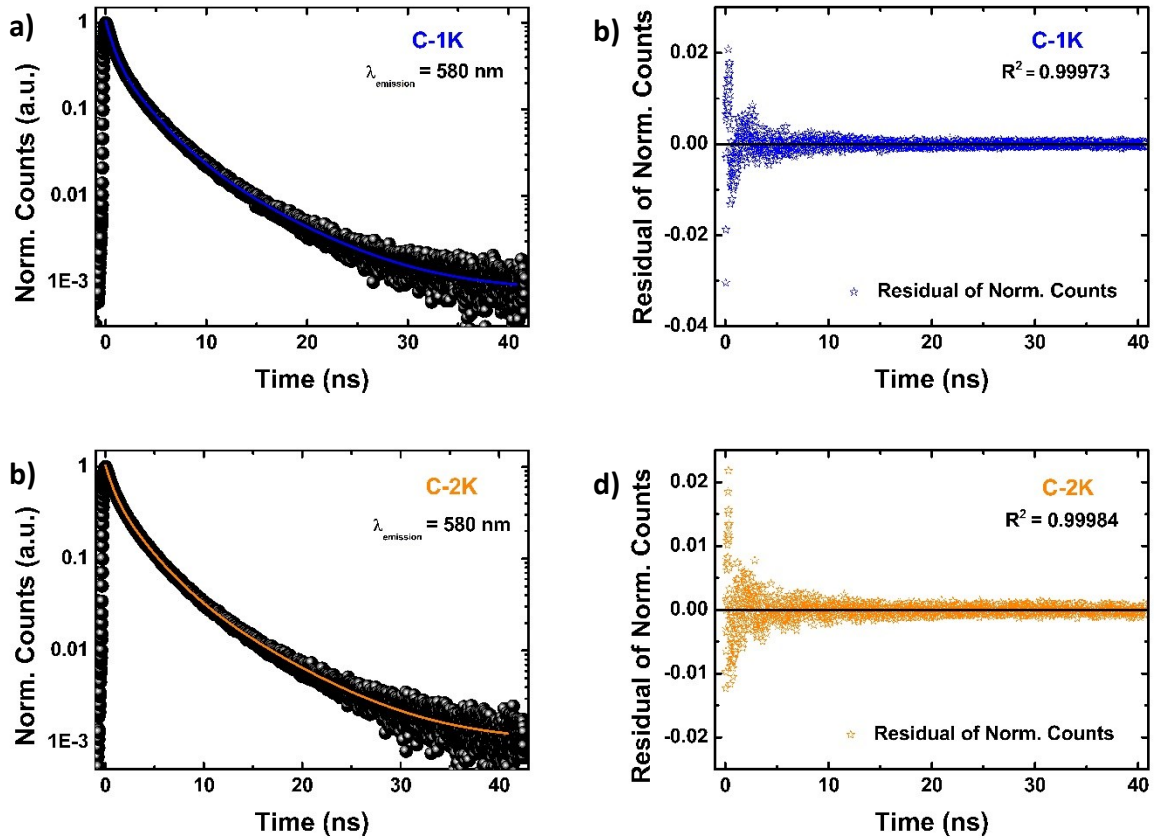


**Figure S21.** The photoluminescence decay traces of KOH-based PDs recorded at 580 nm (left panel) and their corresponding plots of residuals (right panel).

In fact, the tri-exponential fitting model was the most suitable to extract fully the dynamics of photoluminescence, as made evident by relatively high  $R^2$  values, as well as narrow distribution of fitting residuals. Thus-obtained temporal parameters are listed in **Table S3**. In the further step, the weighted averaged decay times ( $\langle\tau\rangle$ ) were calculated by integrating the individual lifetime components and their amplitudes through the following equation:<sup>22</sup>

$$\langle\tau\rangle = \frac{\sum A_i \cdot \tau_i^2}{\sum A_i \cdot \tau_i}$$

where  $\tau_i$  represents lifetime  $i$ -component (ns),  $A_i$  corresponds to a proper normalized amplitude, and  $\langle\tau\rangle$  denotes the calculated average lifetime (ns);

**Table S4.** The dynamic characteristics of photoluminescence for all four PDs samples.

Sample	Emission wavelength (nm)	$\tau_1$ (ns)	Normalized amplitude 1 (%)	$\tau_2$ (ns)	Normalized amplitude 2 (%)	$\tau_3$ (ns)	Normalized amplitude 3 (%)	$\langle\tau\rangle$ (ns)
C-1Na	480	0.92	51%	3.16	44%	8.27	6%	3.73
	580	0.84	49%	2.94	43%	7.26	8%	3.62
C-2Na	480	0.55	35%	2.07	54%	6.19	10%	3.24
	580	0.68	54%	2.48	40%	7.07	7%	3.34
C-1K	480	0.80	48%	2.77	43%	6.60	9%	3.46
	580	0.63	48%	2.26	39%	5.60	12%	3.23
C-2K	480	0.65	43%	2.28	48%	6.94	9%	3.46
	580	0.70	47%	2.43	43%	6.64	10%	3.49

The synergy of PLQY ( $\lambda_{\text{exc.}} = 377 \text{ nm}$ ) and the average lifetime ( $\lambda_{\text{exc.}} = 377 \text{ nm}$ ,  $\lambda_{\text{em.}} = 480 \text{ nm}$ ) allows one to recognize clearly the contribution of radiative and non-radiative transitions, induced due to the excitation in the UV regime. The radiative and non-radiative rate constants were estimated, considering two relations:<sup>23-26</sup>

$$PLQY = \frac{k_r}{k_r + k_{nr}} \quad \langle \tau \rangle = \frac{1}{k_r + k_{nr}}$$

where  $k_r$  and  $k_{nr}$  represent the rate constants of radiative and non-radiative transitions ( $\text{ns}^{-1}$ ), respectively,  $\langle \tau \rangle$  denotes the average photoluminescence decay time (ns);

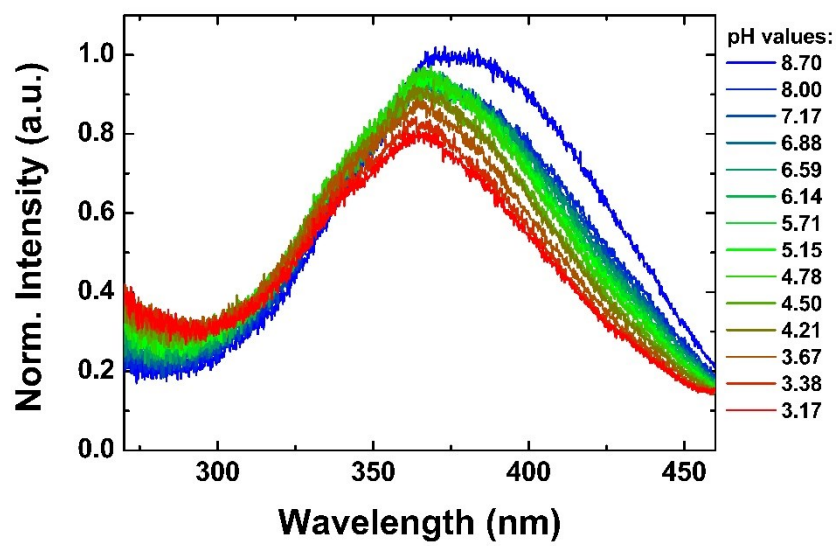


Figure S22. Evolution of excitation spectra in relation to pH values.

## References:

1. Hou, H.; Banks, C. E.; Jing, M.; Zhang, Y.; Ji, X., Carbon Quantum Dots and Their Derivative 3D Porous Carbon Frameworks for Sodium-Ion Batteries with Ultralong Cycle Life. *Adv Mater* **2015**, *27* (47), 7861-6.
2. Silverstein, R. M.; Webster, F. X.; Kiemle, D. J.; Bryce, D. L., *Spectrometric identification of organic compounds*. 2015.
3. Colthup, N. B.; Daly, L. H.; Wiberley, S. E., CHAPTER 9 - CARBONYL COMPOUNDS. In *Introduction to Infrared and Raman Spectroscopy (Third Edition)*, Colthup, N. B.; Daly, L. H.; Wiberley, S. E., Eds. Academic Press: San Diego, 1990; pp 289-325.
4. Colthup, N. B.; Daly, L. H.; Wiberley, S. E., CHAPTER 10 - ETHERS, ALCOHOLS, AND PHENOLS. In *Introduction to Infrared and Raman Spectroscopy (Third Edition)*, Colthup, N. B.; Daly, L. H.; Wiberley, S. E., Eds. Academic Press: San Diego, 1990; pp 327-337.
5. Colthup, N. B.; Daly, L. H.; Wiberley, S. E., CHAPTER 5 - METHYL AND METHYLENE GROUPS. In *Introduction to Infrared and Raman Spectroscopy (Third Edition)*, Colthup, N. B.; Daly, L. H.; Wiberley, S. E., Eds. Academic Press: San Diego, 1990; pp 215-233.
6. Colthup, N. B.; Daly, L. H.; Wiberley, S. E., CHAPTER 8 - AROMATIC AND HETEROAROMATIC RINGS. In *Introduction to Infrared and Raman Spectroscopy (Third Edition)*, Colthup, N. B.; Daly, L. H.; Wiberley, S. E., Eds. Academic Press: San Diego, 1990; pp 261-288.
7. De, B.; Karak, N., A green and facile approach for the synthesis of water soluble fluorescent carbon dots from banana juice. *RSC Advances* **2013**, *3* (22), 8286-8290.
8. Zhu, Y.; Ji, X.; Pan, C.; Sun, Q.; Song, W.; Fang, L.; Chen, Q.; Banks, C. E., A carbon quantum dot decorated RuO<sub>2</sub> network: outstanding supercapacitances under ultrafast charge and discharge. *Energy & Environmental Science* **2013**, *6* (12), 3665-3675.
9. Socrates, G., *Infrared and Raman Characteristic Group Frequencies: Tables and Charts, 3rd Edition*. 2004; p 366.
10. Dutta Choudhury, S.; Chethodil, J. M.; Gharat, P. M.; P. K, P.; Pal, H., pH-Elicited Luminescence Functionalities of Carbon Dots: Mechanistic Insights. *The Journal of Physical Chemistry Letters* **2017**, *8* (7), 1389-1395.
11. Chen, B.; Li, F.; Li, S.; Weng, W.; Guo, H.; Guo, T.; Zhang, X.; Chen, Y.; Huang, T.; Hong, X.; You, S.; Lin, Y.; Zeng, K.; Chen, S., Large scale synthesis of photoluminescent carbon nanodots and their application for bioimaging. *Nanoscale* **2013**, *5* (5), 1967-1971.
12. Colthup, N. B.; Daly, L. H.; Wiberley, S. E., CHAPTER 13 - MAJOR SPECTRA-STRUCTURE CORRELATIONS BY SPECTRAL REGIONS. In *Introduction to Infrared and Raman Spectroscopy (Third Edition)*, Colthup, N. B.; Daly, L. H.; Wiberley, S. E., Eds. Academic Press: San Diego, 1990; pp 387-481.
13. Sun, X.; Li, Y., Colloidal Carbon Spheres and Their Core/Shell Structures with Noble-Metal Nanoparticles. *Angewandte Chemie International Edition* **2004**, *43* (5), 597-601.
14. Tayyari, S. F.; Zeegers-Huyskens, T.; Wood, J. L., Spectroscopic study of hydrogen bonding in the enol form of  $\beta$ -diketones—II. Symmetry of the hydrogen bond. *Spectrochimica Acta Part A: Molecular Spectroscopy* **1979**, *35* (12), 1289-1295.
15. Ogoshi, H.; Nakamoto, K., Normal-Coordinate Analyses of Hydrogen-Bonded Compounds. V. The Enol Forms of Acetylacetone and Hexafluoroacetylacetone. *The Journal of Chemical Physics* **1966**, *45* (8), 3113-3120.

16. Huang, J. J.; Zhong, Z. F.; Rong, M. Z.; Zhou, X.; Chen, X. D.; Zhang, M. Q., An easy approach of preparing strongly luminescent carbon dots and their polymer based composites for enhancing solar cell efficiency. *Carbon* **2014**, *70*, 190-198.
17. Song, Z.; Quan, F.; Xu, Y.; Liu, M.; Cui, L.; Liu, J., Multifunctional N,S co-doped carbon quantum dots with pH- and thermo-dependent switchable fluorescent properties and highly selective detection of glutathione. *Carbon* **2016**, *104*, 169-178.
18. Vallan, L.; Urriolabeitia, E. P.; Ruipérez, F.; Matxain, J. M.; Canton-Vitoria, R.; Tagmatarchis, N.; Benito, A. M.; Maser, W. K., Supramolecular-Enhanced Charge Transfer within Entangled Polyamide Chains as the Origin of the Universal Blue Fluorescence of Polymer Carbon Dots. *Journal of the American Chemical Society* **2018**, *140* (40), 12862-12869.
19. Kwon, W.; Lee, G.; Do, S.; Joo, T.; Rhee, S.-W., Size-Controlled Soft-Template Synthesis of Carbon Nanodots toward Versatile Photoactive Materials. *Small* **2014**, *10* (3), 506-513.
20. Leyre, S.; Coutino-Gonzalez, E.; Joos, J. J.; Ryckaert, J.; Meuret, Y.; Poelman, D.; Smet, P. F.; Durinck, G.; Hofkens, J.; Deconinck, G.; Hanselaer, P., Absolute determination of photoluminescence quantum efficiency using an integrating sphere setup. *Review of Scientific Instruments* **2014**, *85* (12), 123115.
21. Boyer, J.-C.; van Veggel, F. C. J. M., Absolute quantum yield measurements of colloidal NaYF<sub>4</sub>: Er<sup>3+</sup>, Yb<sup>3+</sup> upconverting nanoparticles. *Nanoscale* **2010**, *2* (8), 1417-1419.
22. LeCroy, G. E.; Messina, F.; Sciortino, A.; Bunker, C. E.; Wang, P.; Fernando, K. A. S.; Sun, Y.-P., Characteristic Excitation Wavelength Dependence of Fluorescence Emissions in Carbon “Quantum” Dots. *The Journal of Physical Chemistry C* **2017**, *121* (50), 28180-28186.
23. Hamanaka, Y.; Ozawa, K.; Kuzuya, T., Enhancement of Donor–Acceptor Pair Emissions in Colloidal AgInS<sub>2</sub> Quantum Dots with High Concentrations of Defects. *The Journal of Physical Chemistry C* **2014**, *118* (26), 14562-14568.
24. Valeur, B.; Berberan-Santos, M. N., *Molecular Fluorescence: Principles and Applications*. Wiley: 2013.
25. Lakowicz, J. R., *Principles of Fluorescence Spectroscopy*. 3rd ed.; Springer: Boston, MA, 2006.
26. Lakowicz, J. R., Radiative Decay Engineering: Biophysical and Biomedical Applications. *Analytical Biochemistry* **2001**, *298* (1), 1-24.